To appear in *Transportmetrica B: Transport Dynamics*
Vol. 00, No. 00, Month 20XX, 1–17

Gaussian approximation for modeling traffic flow on a homogeneous road segment

Brian Thomas Vachta[a] †, Xiao Qin[b] * and Jung-Han Kimn[a] ‡

[a]*Department of Mathematics and Statistics, South Dakota State University, Brookings, SD 57007, USA*; [b]*Department of Civil and Environmental Engineering, South Dakota State University, Brookings, SD 57007, USA.*

(*Received 25 July 2014*)

*Corresponding author. Email: xiao.qin@sdstate.edu Phone: 6056886355 † Email: brianvachta@msn.com Phone: 6413309336 ‡ Email: jung-han.kimn@sdstate.edu Phone: 6056885842

A Gaussian approximation of the stochastic model in (Jabari and Liu 2012) proposed in (Jabari and Liu 2013) is implemented for a case study. The Gaussian approximation estimates the mean traffic density from the long term trend of a stochastic model, and a variance calculated from the deviance of the stochastic model and its long term limit. The mean is the deterministic Godunov scheme. Through this case study the model is shown capable of producing accurate queue size estimates in a viable amount of time for cycle-by-cycle traffic estimation on an arterial road. Model variance is controllable by choice of time step; however, smaller time steps limit the ability of the model to produce a range of solutions which contain the ground truth observation.

Keywords: Gaussian approximation; stochastic traffic flow; cell transmission model; homogeneous road segment; macroscopic model; Godunov scheme

1. Introduction

Traffic congestion on roads is a continuing concern around the world. In the past this has been addressed by adding capacity to infrastructure, i.e. adding more lanes to highways and adding more roads. This solution is largely subject to budget constraints.

Another solution which has been adopted more recently is operating existing infrastructure more efficiently. This strategy involves using knowledge of real-time traffic conditions to reduce congestion (Cambridge Systematics and Institute. 2005). Examples of this include ramp metering and advanced wait time notice on freeways. In the context of traffic lights, real-time traffic data allows for more efficient traffic signal timings.

Traffic signals historically operate by fixed cycle lengths of red time and green time. Recently, many fixed cycle lengths require actuation in order for certain phases of the traffic cycle to occur i.e. left turn signals that are only included in the cycle is a vehicle is detected in the left turn lane. Actuated signals can be more efficient than fixed cycle timings by skipping unnecessary phases of a signal cycle, shortening the time vehicles wait at the signal. However traffic has to stop at the stop line in order to actuate the signal. Adaptive (predictive) traffic signal timings, which are based on real-time arrival rates of traffic, further improve efficiency by optimizing signal cycle lengths according to expected queue sizes (number of vehicles stopped behind stop line). The expected queue sizes identify where the bulk of traffic is located. As an example, if the location of the bulk of traffic is located, that traffic could progress through continual green lights.

In the development of cost-efficient methods to predict traffic conditions, point-source detectors such as inductance loop detectors are cheaper to implement; however, they lack the accuracy that video cameras have. This has led to the development of traffic flow models to predict traffic conditions based off of inductance loop detector data.

1.1. *Traffic modeling overview*

Traffic flow theory models estimate traffic evolution for various levels of vehicle aggregation. The most common types of models are microscopic, mesoscopic, and macroscopic.

Microscopic traffic flow models have high detail and depend on driver's behavior interaction between individual vehicles. These behaviors include driver's choice of time distance between other vehicles, choice of speed, acceleration, deceleration, and lane changes. Microscopic models can simulate complex traffic conditions. In order to accurately model traffic, a large amount of parameters are required. A disadvantage to using microscopic models to predict traffic conditions is that real-time point-source data is usually aggregated over one to five minute intervals, thus model updates are not as precise when updated with aggregated data.

Mesoscopic models have medium detail, describing the behavior of small groups of vehicles, segregated by speed and position.

Macroscopic models have low level of detail as they represent aggregated levels of flow without considering individual vehicle behavior. These models are able to produce results fast and are able to use aggregated real-time data without loss of accuracy, which motivates their application.

Lighthill and Whitham (Lighthill and Whitham 1955), and Richards (Richards 1956) proposed a first-order deterministic model which is widely used throughout macroscopic modeling (LWR model). The LWR model has been used to describe queue buildup and discharge in traffic. It shows the existence of shock waves in traffic; however, its solutions assume that traffic can adjust its speed instantaneously. It lacks diffusive terms which would model drivers' reaction to changes in traffic such as shock waves.

While deterministic models have been able to capture important physical phenomenon,

these models are typically dependent on an assumed flow-density relationship. Flow-density relationships admit large fluctuations in behavior as shown in (Kim and Zhang 2008; Sumalee et al. 2011). This high variability is due to driver decisions, adverse weather conditions, etc. and has led to the development of stochastic microscopic and macroscopic models to capture this variation. A challenge in stochastic modeling is obtaining reasonable computation times. In an attempt to minimize this issue, many models have been created by adding Gaussian noise to deterministic models. Since Gaussian noise can be characterized by its mean and variance, this becomes less of a computational hassle. However the addition of Gaussian noise could contradict physical phenomenon by producing negative traffic densities as well as avoiding mean dynamics of the original deterministic model as the dynamic equations are nonlinear (Jabari and Liu 2012).

A computationally viable model is proposed in (Jabari and Liu 2013) which uses the the long term trend of the stochastic Markovian model in (Jabari and Liu 2012) as the mean of the model. The covariance of the mean is derived from the deviance of the stochastic model and its deterministic long term limit. The long term trend or fluid limit of the stochastic model is the deterministic Godunov scheme, which is a method for solving the macroscopic LWR model. The variance is controllable by the time step such that non-negative densities ranges can be obtained for sufficiently small time step.

Because of the linearity of the stochastic model, the state can be compared to real data using the linear Kalman filter to improve mean traffic density estimations. Using the linear Kalman filter is faster than using non-linear filters and is a unique feature of this model.

1.2. *Objective*

The primary objective of this paper is to investigate the use of the Gaussian approximation proposed in (Jabari and Liu 2012). This method is chosen for its ability to guarantee of non-negative traffic flow and that the variance is derived from deterministic model parameters such that the model is computationally feasible to implement in traffic control systems. We implement the model for a case study in which we wish to describe traffic conditions downstream on a homogeneous road with no lane changes from knowledge of upstream conditions.

2. Literary review

2.1. *Lighthill, Whitham, and Richards model*

Macroscopic models describe traffic evolution as aggregated amounts of traffic. These models use traffic density, flow rates, and a fundamental relationship to characterize traffic. Lighthill and Whitham (Lighthill and Whitham 1955), and Richards (Richards 1956) proposed the following first-order macroscopic model from hydrodynamic theory:

$$\rho_t + q_x = 0, \tag{1}$$

for traffic density $\rho(x,t)$, and flow $q(x,t)$. This partial differential equation (PDE) represents the change of vehicles in a road segment as the difference of the flow of vehicles in and out of the road. This was proposed as a model of traffic flow with the assumption that of the existence of a flux function: $q(x,t) = Q(\rho(x,t))$. This reduces the PDE to an

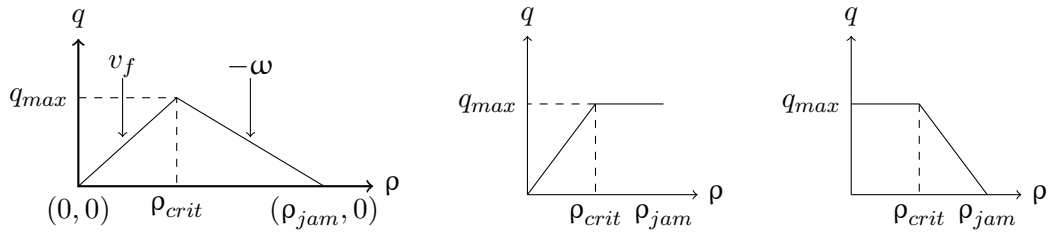

(a) Triangular Fundamental Diagram (b) Sending function (c) Receiving function

Figure 1.: Example of Daganzo's flux function (a) composed from the minimum of a sending function (b) and a receiving function (c).

ordinary differential equation:

$$\frac{\partial \rho(x,t)}{\partial t} + Q'(\rho)\frac{\partial \rho(x,t)}{\partial x} = 0. \tag{2}$$

The general solutions to equation 2 are a family of straight lines in the $x-t$ plane. Each solution has wave speed, or slope, $Q'(\rho)$ characterized by the value of ρ. A popular method to model traffic with the LWR model is to divide a road into segments called cells, choose a flux function, and use initial conditions to solve 2. By dividing the road into cells, the assumption of differentiability used to derive 2 does not hold, and only weak solutions are allowed. The weak solutions are not unique, such that various methods have been developed to physically model traffic flow. These methods are based on how shock waves and expansion waves are demonstrated.

Daganzo (Daganzo 1994, 1995) proposed piecewise linear sending and receiving functions in equations 3 and 4 as flux functions to describe flow between cells as well as shock waves in traffic. These functions are used to create a flux function as seen in Figure 1. This method is a cell transmission model (CTM), which is a special case of Godunov's scheme (Godunov 1959). Daganzo's cell transmission model was developed to solve the LWR model for complicated network topologies.

$$S_e(\rho(i,t)) = \min\{v_f\rho(i,t), q_{max}\} \tag{3}$$

$$R_e(\rho(i,t)) = \min\{q_{max}, \omega(\rho_{jam} - \rho(i,t))\} \tag{4}$$

The subscript 'e' denotes an equilibrium or empirically derived (fundamental) flow-density relationship.

For ease of notation, we declare $\boldsymbol{y}(i+.5,t)$ to be the vector of densities in cells adjacent to the boundary at $i+.5$ at time t for all $i \in \mathcal{C}$.

$$\boldsymbol{y}(i+.5,t) = \begin{bmatrix} \rho(i,t) \\ \rho(i+1,t) \end{bmatrix} \tag{5}$$

This notation is used in calculation of CTM flux functions, which calculate shock waves at the boundaries of cells. $|\mathcal{C}|$ denotes the cardinality, or size of the set of cells in $\mathcal{C}$. This is used to denote the index of the last cell. The procedure for Daganzo's CTM is found in Algorithm 1.

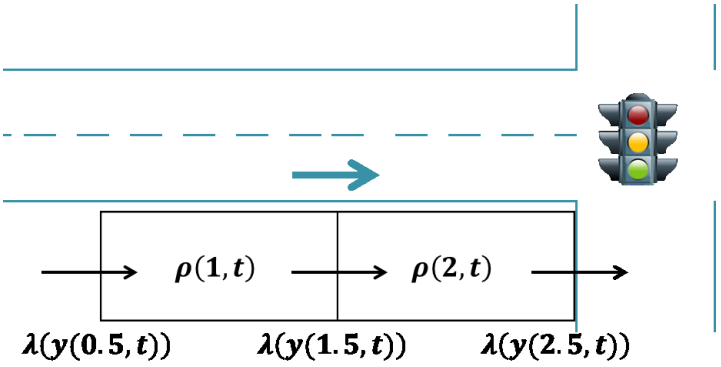

Figure 2.: Cell transmission model with two cells.

Algorithm 1 Cell Transmission Model

Assume initial density $\rho(i,0)$ for all cells $i \in \mathcal{C}$.
Initialize model with fundamental parameters.
Compute flux function at boundaries for each cell $i = 1$ to $|\mathcal{C}|$ from $k = 1$ to end:

$$\lambda(\boldsymbol{y}(.5,t_k)) = R_e(\rho(1,t_k))$$
$$\lambda(\boldsymbol{y}(|\mathcal{C}|+.5,t_k)) = S_e(\rho(|\mathcal{C}|,t_k))$$
$$\lambda(\boldsymbol{y}(i+.5,t_k)) = \min\{S_e(\rho(i,t_k), R_e(\rho(i+1,t_k)\}$$

Update new densities:

$$\rho(i,t_{k+1}) = \rho(i,t_k) + \frac{\Delta t}{\ell_i}(\lambda(\boldsymbol{y}(i-.5,t_k) - \lambda(\boldsymbol{y}(i+.5,t_k))$$

Next k

3. Gaussian approximation

The Gaussian approximation model uses the cell transmission model as an approximation to the long term trend of the stochastic model in (Jabari and Liu 2012). The stochastic model is a microscopic queueing model which counts vehicle departures from cells based on stochastic time headways. The deviance between the stochastic and its fluid limit, outlined in (Jabari and Liu 2013), allows us to calculate the covariance of the deterministic model based on the stochastic model's probabilistic deviance from it. This allows a range of solutions to be given for density estimates based on a stochastically derived model. The deviance is derived as a stochastic differential equation, with solution in differential form given in 6 for initial covariance matrix $\boldsymbol{\Psi}(0)$, where $\mathbf{D}(t), \mathbf{B}$, and $\boldsymbol{\Gamma}(t)$ are given in 9, 10, and 11. Equation 6 is approximated using Riemann sum integration:

$$\frac{d\boldsymbol{\Psi}(t)}{dt} = \mathbf{D}(t)\boldsymbol{\Psi}(t) + \boldsymbol{\Psi}(t)\mathbf{D}(t)^T + \mathbf{B}\boldsymbol{\Gamma}(t)\boldsymbol{\Gamma}(t)^{\mathbf{T}}\mathbf{B}^{\mathbf{T}} \tag{6}$$

$$\begin{aligned}\int_t^{t+\Delta t} \frac{d\boldsymbol{\Psi}(t)}{dt}\,dt &= \boldsymbol{\Psi}(t+\Delta t) - \boldsymbol{\Psi}(t) \\ &\simeq \mathbf{D}(t)\boldsymbol{\Psi}(t)\Delta t + \boldsymbol{\Psi}(t)\mathbf{D}(t)^T\Delta t + \mathbf{B}\boldsymbol{\Gamma}(t)\boldsymbol{\Gamma}(t)^{\mathbf{T}}\mathbf{B}^{\mathbf{T}}\Delta t\end{aligned} \tag{7}$$

Such that:

$$\mathbf{\Psi}(t+\Delta t) \simeq \mathbf{\Psi}(t) + \mathbf{D}(t)\mathbf{\Psi}(t)\Delta t + \mathbf{\Psi}(t)\mathbf{D}(t)^T\Delta t + \mathbf{B}\mathbf{\Gamma}(t)\mathbf{\Gamma}(t)^{\mathbf{T}}\mathbf{B}^{\mathbf{T}}\Delta t. \tag{8}$$

This solution serves as the covariance of the data in the cells. The diagonal elements of the covariance matrix are the individual variances of each corresponding cell's density.

$\mathbf{D}(t)$ is defined to be a $|\mathcal{C}| \times |\mathcal{C}|$ matrix with row elements given by 9 for each cell $i \in \mathcal{C}$. The middle element is the diagonal element of row i,

$$\frac{1}{\ell_i}\left[\dots 0 \ \frac{\partial\lambda(\bar{\boldsymbol{y}}(i-.5,t))}{\partial\bar{\rho}(i-1,t)} \ \frac{\partial\lambda(\bar{\boldsymbol{y}}(i-.5,t))}{\partial\bar{\rho}(i,t)} - \frac{\partial\lambda(\bar{\boldsymbol{y}}(i+.5,t))}{\partial\bar{\rho}(i,t)} \ -\frac{\partial\lambda(\bar{\boldsymbol{y}}(i+.5,t))}{\partial\bar{\rho}(i+1,t)} \ 0 \dots\right]. \tag{9}$$

B is a $|\mathcal{C}| \times |\mathcal{C}| + 1$ matrix used to correctly combine flux terms in $\mathbf{\Gamma}(t)$ with the corresponding cell length,

$$\mathbf{B} \equiv \begin{bmatrix} \frac{1}{\ell_1} & -\frac{1}{\ell_1} & 0 & 0 & \dots & 0 & 0 \\ 0 & \frac{1}{\ell_2} & -\frac{1}{\ell_2} & 0 & \dots & 0 & 0 \\ \vdots & \ddots & \ddots & \ddots & \ddots & \ddots & \vdots \\ 0 & 0 & \dots & 0 & 0 & \frac{1}{\ell_{|\mathcal{C}|}} & -\frac{1}{\ell_{|\mathcal{C}|}} \end{bmatrix}. \tag{10}$$

$\mathbf{\Gamma}(t)$ is a $|\mathcal{C}| + 1 \times |\mathcal{C}| + 1$ matrix of Itô integrands

$$\mathbf{\Gamma} \equiv \begin{bmatrix} \bar{c}\sqrt{\lambda(\bar{\boldsymbol{y}}(.5,t))} & 0 & \dots & 0 \\ 0 & \bar{c}\sqrt{\lambda(\bar{\boldsymbol{y}}(1.5,t))} & \dots & 0 \\ \vdots & \ddots & \ddots & \vdots \\ 0 & \dots & 0 & \bar{c}\sqrt{\lambda(\bar{\boldsymbol{y}}(|\mathcal{C}|+.5,t))} \end{bmatrix}. \tag{11}$$

3.1. *Derivatives of flux functions*

The matrix $\mathbf{D}(t)$ requires the computation of partial derivatives of flux functions, which are non-differentiable in the classical sense. We can rewrite flux equation in Algorithm 1 as the average of the sending and receiving functions minus the distance (norm) between the two:

$$\min\{S_e(\bar{\rho}_i), R_e(\bar{\rho}_{i+1})\} = \frac{1}{2}\left(S_e(\bar{\rho}_i) + R_e(\bar{\rho}_{i+1}) - |S_e(\bar{\rho}_i) - R_e(\bar{\rho}_{i+1})|\right) \tag{12}$$

$$= \frac{1}{2}\left(S_e(\bar{\rho}_i) + R_e(\bar{\rho}_{i+1}) - \sqrt{(S_e(\bar{\rho}_i) - R_e(\bar{\rho}_{i+1}))^2}\right), \tag{13}$$

for $\bar{\rho}_i, \bar{\rho}_{i+1} \in [0, \rho_{jam}]$. This allows the partial derivatives to be written:

$$\frac{\partial\lambda(\bar{\boldsymbol{y}}(i+.5))}{\partial\rho_i} = \frac{1}{2}\frac{dS_e(\bar{\rho}_i)}{d\rho_i}\left(1 - \frac{S_e(\bar{\rho}_i) - R_e(\bar{\rho}_{i+1})}{|S_e(\bar{\rho}_i) - R_e(\bar{\rho}_{i+1})|}\right) \tag{14}$$

$$\frac{\partial\lambda(\bar{\boldsymbol{y}}(i+.5))}{\partial\rho_{i+1}} = \frac{1}{2}\frac{dR_e(\bar{\rho}_{i+1})}{d\rho_{i+1}}\left(1 + \frac{S_e(\bar{\rho}_i) - R_e(\bar{\rho}_{i+1})}{|S_e(\bar{\rho}_i) - R_e(\bar{\rho}_{i+1})|}\right). \tag{15}$$

Table 1.: Flux derivatives

	$S_e(\bar{\rho}_i) < R_e(\bar{\rho}_{i+1})$	$S_e(\bar{\rho}_i) = R_e(\bar{\rho}_{i+1})$	$S_e(\bar{\rho}_i) > R_e(\bar{\rho}_{i+1})$
$\frac{\partial\lambda(\bar{\boldsymbol{y}}(i+.5))}{\partial\rho_i}$	$\frac{dS_e(\bar{\rho}_i)}{d\rho_i}$	$\frac{1}{2}\frac{dS_e(\bar{\rho}_i)}{d\rho_i}$	0
$\frac{\partial\lambda(\bar{\boldsymbol{y}}(i+.5))}{\partial\rho_{i+1}}$	0	$\frac{1}{2}\frac{dR_e(\bar{\rho}_{i+1})}{d\rho_{i+1}}$	$\frac{dR_e(\bar{\rho}_{i+1})}{d\rho_{i+1}}$

The partial derivatives exist everywhere except for $S_e(\bar{\rho}_i) = R_e(\bar{\rho}_{i+1})$. For this case, equation 12 reduces to:

$$\min\{S_e(\bar{\rho}_i), R_e(\bar{\rho}_{i+1})\} = \frac{1}{2}\left(S_e(\bar{\rho}_i) + R_e(\bar{\rho}_{i+1})\right), \tag{16}$$

such that the partial derivatives are:

$$\frac{\partial\lambda(\bar{\boldsymbol{y}}(i+.5))}{\partial\rho_i} = \frac{1}{2}\frac{dS_e(\bar{\rho}_i)}{d\rho_i} \tag{17}$$

$$\frac{\partial\lambda(\bar{\boldsymbol{y}}(i+.5))}{\partial\rho_{i+1}} = \frac{1}{2}\frac{dR_e(\bar{\rho}_{i+1})}{d\rho_{i+1}}. \tag{18}$$

A summary of the weak partial derivatives of the flux function are found in Table 1.

3.2. *Gaussian Approximation algorithm*

Algorithm 2 Gaussian Approximation

Initialize model with fundamental parameters and B:

$$\bar{\rho}(\cdot, 0) = 0$$
$$\lambda(\bar{\boldsymbol{y}}(\cdot, 0) = 0$$

For $k = 1$ to end:
Compute flux function at boundaries for $i = 1$ to $|\mathcal{C}| - 1$:

$$\lambda(\bar{\boldsymbol{y}}(.5, t_k)) = R_e(\bar{\rho}(1, t_k))$$
$$\lambda(\bar{\boldsymbol{y}}(|\mathcal{C}| + .5, t_k)) = S_e(\bar{\rho}(|\mathcal{C}|, t_k))$$
$$\lambda(\bar{\boldsymbol{y}}(i + .5, t_k)) = \min\{S_e(\bar{\rho}(i, t_k), R_e(\bar{\rho}(i+1, t_k)\}$$

Update $\boldsymbol{\Gamma}(t), \mathbf{D}(t)$.
Compute covariance:

$$\boldsymbol{\Psi}(t_{k+1}) = \boldsymbol{\Psi}(t_k) + \mathbf{D}(t_k)\boldsymbol{\Psi}(t_k)\Delta t + \boldsymbol{\Psi}(t_k)\mathbf{D}(t_k)^T\Delta t + \mathbf{B}\boldsymbol{\Gamma}(t_k)\boldsymbol{\Gamma}(t_k)^{\mathbf{T}}\mathbf{B}^{\mathbf{T}}\Delta t$$

Algorithm 2 Gaussian Approximation (continued)

Update mean densities for $i = 1$ to $|\mathcal{C}|$:

$$\bar{\rho}(i, t_{k+1}) = \bar{\rho}(i, t_k) + \frac{\Delta t}{\ell_i}(\lambda(\bar{\boldsymbol{y}}(i - .5, t_k) - \lambda(\bar{\boldsymbol{y}}(i + .5, t_k))$$

Calculate confidence interval from variance and mean:

$$ci^+ = \bar{\rho}(i, t_{k+1}) + 1.96\sqrt{\boldsymbol{\Psi}_{ii}(t_{k+1})\Delta t}$$
$$ci^- = \bar{\rho}(i, t_{k+1}) - 1.96\sqrt{\boldsymbol{\Psi}_{ii}(t_{k+1})\Delta t}$$

3.3. *Non-negative densities*

The diagonal elements of the covariance matrix are the variances for each cell density. The variance is used to create a confidence interval about the mean. Mean density values are automatically guaranteed to be non-negative by the calculation of flux between cells. The range of potential density values around the mean is not guaranteed to be non-negative.

We know from (Jabari and Liu 2013) that the covariance matrix converges to $\mathbf{B\Gamma\Gamma^T B^T}dt$ for which, the diagonal elements are $\boldsymbol{\Psi}_{ii} = \left(\frac{\bar{c}}{\ell_i}\right)^2 (\lambda(\bar{y}(i-1,t))+\lambda(\bar{y}(i,t)))dt$. The variance is then calculated by:

$$\begin{aligned}\int_t^{t+\Delta t} \left(\frac{\bar{c}}{\ell_i}\right)^2 (\lambda(\bar{y}(i-1,u)) + \lambda(\bar{y}(i,u)))du &= \int_t^{t+\Delta t} \mathbb{E}|\tilde{\rho}(i,u) - \mathbb{E}\tilde{\rho}(i,u)|^2 du \\ &= \left(\frac{\bar{c}}{\ell_i}\right)^2 (\lambda(\bar{y}(i-1,t)) + \lambda(\bar{y}(i,t)))\Delta t \\ &= \boldsymbol{\Psi}_{ii}\Delta t.\end{aligned} \tag{19}$$

To control the range of solutions to be guaranteed non-negative with 95% confidence, one would choose the smallest of the time steps that satisfies the CFL condition (Leveque 1992) and $\bar{\rho} - 1.96\sqrt{\boldsymbol{\Psi}_{ii}\Delta t} \geq 0$. For the latter part of the condition we have:

$$\Delta t \leq \frac{\bar{\rho}^2}{(1.96\sqrt{\boldsymbol{\Psi}_{ii}})^2}. \tag{20}$$

If traffic is in a free flow state such that $S_e(\bar{\rho}) < R_e(\bar{\rho})$, we have:

$$\begin{aligned}\Delta t &\leq \frac{\bar{\rho}^2 \ell_i^2}{7.68\bar{c}^2 v_f \bar{\rho}} \\ &= \frac{\bar{\rho}\ell_i^2}{7.68\bar{c}^2 v_f} \geq \frac{1}{8}\frac{\bar{\rho}\ell_i}{\bar{c}^2}\frac{\ell_i}{v_f}.\end{aligned} \tag{21}$$

The other issue of concern is avoiding densities within the 95% confidence interval that would be greater than jam density ρ_{jam}. This would require $\bar{\rho} + 1.96\sqrt{\boldsymbol{\Psi}_{ii}\Delta t} \leq \rho_{jam}$,

such that

$$\Delta t \leq \frac{(\rho_{jam} - \bar{\rho})^2}{(1.96\sqrt{\boldsymbol{\Psi}_{ii}})^2}. \tag{22}$$

If traffic is in a congested state such that $S_e(\bar{\rho}) > R_e(\bar{\rho})$, we have:

$$\Delta t \leq \frac{(\rho_{jam} - \bar{\rho})\ell_i^2}{7.68\bar{c}^2\omega}. \tag{23}$$

In general, the recommendation in 23 is a more relaxed bound than in 21 as it is often true that $v_f > \omega$. If one wanted to guarantee with 95% confidence that density values around the mean density of $\bar{\rho} = \rho_{crit}$, which is the upper bound of density values which result in $S_e(\bar{\rho}) > R_e(\bar{\rho})$, it would be required that:

$$\Delta t \leq \min\left(\frac{1}{8}\frac{q_{max}}{v_f}\frac{\ell_i^2}{\bar{c}^2 v_f}, \frac{\ell_i}{v_f}\right). \tag{24}$$

Of course, this will cannot guarantee all traffic densities to be non-negative.

3.4. *Numerical example*

The purpose of this example is to show how we implemented the Gaussian approximation model in Algorithm 2 with a 95% confidence interval as allowed by the computation of the covariance matrix. To exhibit queue build-up and discharge by the model, we shall consider a large inlet cell arrival rate $A_{max}(t)$. In actual implementation of the model, the arrival flow rate varies with real-time data calibration. Consider an arterial road with a traffic signal that turns red, $g(t) = 0$ for $t \in [30, 150)$ and is green otherwise $g(t) = 1$ is modeled for 250 seconds. We choose to model this as a simple two cell setting with a cell length of .05km. Assume a triangular fundamental relationship with free-flow speed $v_f = 100$km/hr, maximum flow rate $q_{max} = 2100$veh/hr, backward wave propagation speed $\omega = 14$km/hr, and jam density $\rho_{jam} = 171$veh/km, coefficient of variation $\bar{c} = 1$ for both states, maximum arrival rate $A_{max}(t) = 2100$, and a time step of $\Delta t = .045$ seconds. Then the flux function is calculated as:

$$\lambda(\bar{\boldsymbol{y}}(0.5, t)) = \min\{A_{max}(t), 14(171 - \rho(1, t))\} \tag{25}$$

$$\lambda(\bar{\boldsymbol{y}}(1.5, t)) = \min\{100\rho(1, t), 2100, 14(171 - \rho(2, t))\} \tag{26}$$

$$\lambda(\bar{\boldsymbol{y}}(2.5, t)) = \min\{100\rho(2, t), 2100g(t)\}. \tag{27}$$

$$B = \begin{bmatrix} 20 & -20 & 0 \\ 0 & 20 & -20 \end{bmatrix} \tag{28}$$

$$\boldsymbol{\Gamma}(t) = \begin{bmatrix} \sqrt{\lambda(\bar{\boldsymbol{y}}(.5, t))} & 0 & 0 \\ 0 & \sqrt{\lambda(\bar{\boldsymbol{y}}(1.5, t))} & 0 \\ 0 & 0 & \sqrt{\lambda(\bar{\boldsymbol{y}}(2.5, t))} \end{bmatrix} \tag{29}$$

$$D = \begin{bmatrix} \frac{1}{20}\frac{\partial\lambda(\bar{\boldsymbol{y}}(.5, t))}{\partial\bar{\rho}(1, t)} - \frac{1}{20}\frac{\partial\lambda(\bar{\boldsymbol{y}}y(1.5, t))}{\partial\bar{\rho}(1, t)} & -\frac{1}{20}\frac{\partial\lambda(\bar{\boldsymbol{y}}y(1.5, t))}{\partial\bar{\rho}(2, t)} \\ \frac{1}{20}\frac{\partial\lambda(\bar{\boldsymbol{y}}(1.5, t))}{\partial\bar{\rho}(1, t)} & \frac{1}{20}\frac{\partial\lambda(\bar{\boldsymbol{y}}(1.5, t))}{\partial\bar{\rho}(2, t)} - \frac{1}{20}\frac{\partial\lambda(\bar{\boldsymbol{y}}(2.5, t))}{\partial\bar{\rho}(2, t)} \end{bmatrix} \tag{30}$$

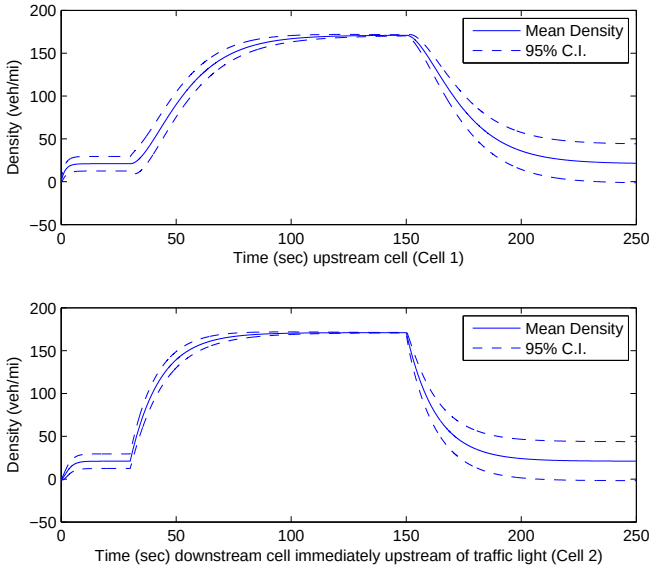

Figure 3.: Traffic densities with 95% confidence intervals.

4. Case Study

An arterial road case study was carried out on eastbound Highway 14 in Brookings, SD between 22nd Ave. and 25th Ave. Data was collected from 7:30am-8:00am and the traffic largely consisted of passenger vehicles, with minimal amounts of lane changing. The road section is homogeneous, which allows us to use a homogeneous conservation equation.

To model traffic conditions on the road, we need to fit the parameters of the triangular fundamental diagram in Figure 1 to traffic conditions specific to the road. We desire to update the model with traffic flow and density data, and hence need to measure traffic conditions upstream. As a measure of performance, we also need to measure the traffic conditions downstream to test model estimates. The maximum queue size is measured downstream to compare with model estimates of density. Density values are used to estimate the queue size.

A video camera recorded the eastbound flow of traffic downstream from the traffic signal at 22nd Ave. at a point at which vehicles have reached free flow speed. The intention being to record the flow and density rates of traffic flow upstream.

The density upstream was measured using the space-mean-speed along with the relation $q = \rho v$ such that:

$$\bar{\rho} = \frac{\frac{1}{\Delta t}\sum_{i=1}^{N} \tau_i}{\Delta x} \tag{31}$$

where τ_i represents the trajectory of vehicle i. Vehicle trajectories times were measured over the length of the upstream segment and segmented by the offset cycle times. Offset in this scenario is the travel time of a vehicle from the detector location to the downstream

Figure 4.: (Daft Logic 2014)

traffic light. Vehicle time trajectories allow density to be calculated over the entire cycle time, just as a inductance loop detector would record vehicle occupancy over an entire cycle length.

Flow rates are taken to be the vehicle count over the offset cycle time. A fixed point in the video is used to count vehicles with.

The Gaussian approximation model is a linear model, which allows it to be calibrated with real-time observations using the linear Kalman filter. This provides an advantage over other filters in that it is relatively fast. The filter is used in this case study to create optimal estimates of upstream density, $\rho(1,t)$, and inlet arrival flow rates, $\mathcal{A}_{max}$.

Another video camera recorded the downstream queue. This camera serves as the ground truth queue size to compare against the model's prediction. The model uses the upstream data to calibrate model estimates with the linear Kalman filter. The model then makes predictions of density for downstream cells. The density for each cell will then be used to determine if the traffic is considered to be in the queue. Cells are considered to be in the queue, starting from the most downstream cell, if the mean traffic speed is less than 8.05km/hr and the cell downstream is also in the queue.

Free flow speed v_f, which is the slope of the free flow regime in Figure 1, is assumed to be a bit larger than the speed limit: $56.32+3.21$km/hr. The capacity flow q_{cap} is determined from the saturation flow rate according to the procedure in (Currin 2001). The jam density ρ_{jam} is estimated by dividing the number of cars in a queue by the estimated length of the queue. The backward wave speed is derived as: $\omega = \dfrac{-q_{cap}}{\rho_{jam} - \rho_{cap}}$. This is the last of the parameters from the fundamental diagram that need to be determined.

The last model parameter we wish to find is the coefficient of variation of vehicle time headways, $\bar{c}$, from the fit of a lognormal distribution to time headways in both the congested and uncongested regimes. Data is fit to 3-parameter lognormal distributions using SAS with parameters in Table 2.

The null hypothesis is that the data are random samples from the assumed distribution. We use Anderson-Darling (A^2) goodness of fit test to test the alternative hypothesis, which is that the data are not from the assumed distribution. The A^2 test values in Table 2 are under their respective critical values for the 0.05 significance levels, thus the distributions fit well enough that we fail to reject the null hypothesis.

A time step of 1/2 of the recommendation of the CFL condition is arbitrarily chosen as the largest time step which visually maintains stability (CFL condition is a *necessary* but not *sufficient*). A time step of this size does not guarantee non-negative density

Table 2.: Lognormal fit to time headways

	Threshold	Scale	Shape	Mean	Std. Dev.	$\bar{c}$	A^2 test
Free Flow	0.5869	0.6485	0.8867	3.420	3.097	0.906	0.4273
Congested	3.252	1.021	1.228	9.154	11.07	1.21	0.3707

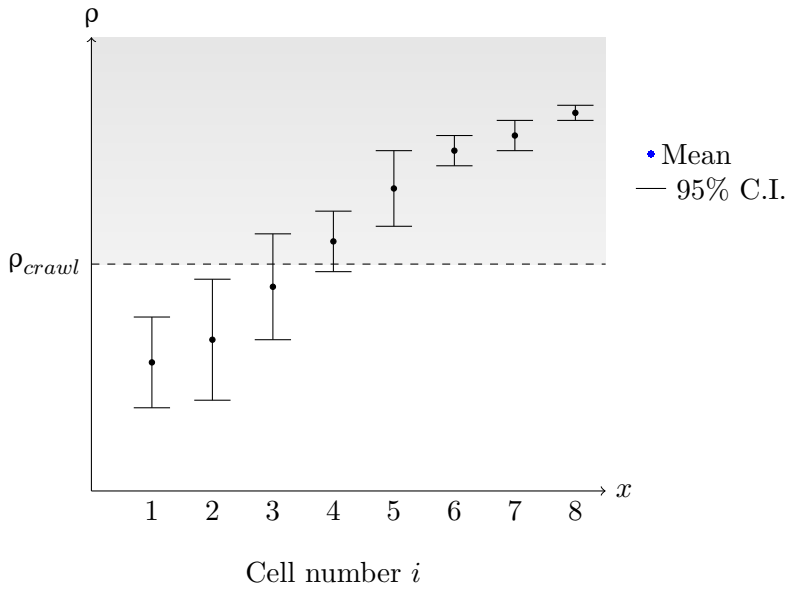

Figure 5.: Densities in gray shaded region considered for maximum queue size

estimates for the confidence interval. A smaller time step of 1/16 of the CLF recommendation, which maintains mostly non-negative density confidence intervals, is shown for comparison.

The choice of cell size affects both accuracy and computation time. From an accuracy standpoint, smaller cell sizes increase the accuracy of the end of the queue. Cell sizes could be as small as the length of a vehicle. The total length of the observed section of road is approximately 248m. The cell size was taken to be factors of the imperial road length.

In selecting the maximum queue from the model, the mean maximum queue size is used as the criteria. Cell densities consecutively above crawl density are considered for the maximum queue size confidence interval. Figure 5 represents an example of a case in which some cells would be considered part of the queue for the confidence interval, but not for the mean, and vice versa. The last five cells would be used in calculation of the maximum density, whereas only the last four cells would be considered for the lower confidence interval. Scenarios arise in which no density for the lower confidence interval are included in the queue size estimate, in which case the lower confidence interval for the maximum queue size is 0 vehicles.

The queue size is determined to be the number of consecutive vehicles from the stop line traveling slower than crawl speed (taken to be $v_{crawl} = 8.05$km/hr). Since the model produces estimates of density, cells are considered to be in the queue if their density is greater than the crawl density. Crawl density is determined to be where the lines $q_{crawl} = v_{crawl}\rho_{crawl}$ and $q = \omega(\rho_{jam} - \rho)$ intersect.

Minimal lane changing occurs in the data set, thus the lanes are independent of each other and can be modeled individually. The queue sizes for the median lane were too small to determine model parameters from and thus is excluded in estimation. Queue sizes for the shoulder lane range from 0 to 10 vehicles.

4.1. *Results*

Results of the model estimates are shown in Figure 6 against the measured queue size. The model uses the first three iterations as a warm-up period to adapt to inlet flow and density values, and these are excluded from the figure.

Since the time step in equation 20 requires knowledge of $\bar{\rho}$ and $\mathbf{\Psi}$, it is difficult to choose a time step greater than zero that will guarantee non-negative density estimates. Additionally, we would not expect a confidence interval that is small enough to avoid non-negative densities to also include measured conditions downstream. One purpose of developing a 95% confidence interval is to capture the range of values that could be expected in the downstream queue.

It is notable that the measurements are close to this range of values. It is also notable how much difference exists in model success for varying cell lengths and time step. Essentially confidence intervals can be constructed for a model with equal cell lengths which produce very different results, as is seen between Figures 6(a) and 6(b). This is because the stochastic model converges to the mean for smaller time steps, and the deviance of the two is what characterizes the 95% confidence interval. Choice of cell size affects the confidence interval as well. The time step decreases by the square of the cell length as the cell length decreases. This results in a conundrum in which a cell length is desired to be small enough to accurately capture the edge of the queue, but large enough such that the confidence interval provides usable information.

The measured observations are not all within the 95% confidence interval for any one model. We tested crawl speeds of 8.05 ± 3.22km/hr to determine if discrepancy existed for determining queue size during observation. Observed vehicles were only considered to be part of the queue if their speed was thought to be less than $v_{crawl} = 8.05$km/hr; however, this was not directly calculated. It could be possible that a vehicle was not observed to be in the queue, but would have been modeled. Results for the model estimate with crawl speeds of 8.05 ± 3.22km/hr did not improve the model's success.

Another possible explanation is error in data collection. While minimal lane changes occur in the videos, a short section of the road between the cameras' view was not observed. Unaccounted lane changes would affect queue size. In estimating the saturation flow rate, few queues were observed with the recommended initial queue of 10 vehicles. Thus the saturation flow rate could be inaccurate. Additionally, this would impact the value of the backwards wave speed ω. The degree of accuracy in measurements of distance and time in videos can affect the accuracy of the all of the data as well.

Throughout this case study, many updates were made to the data to improve their accuracy. The changes that the model was most sensitive to were changing the upstream flow rates and changing the free flow speed and backward wave speed. This emphasizes the importance of fitting the fundamental parameters to relevant historical data.

Updating density values resulted in negligible change, as is expected for a Markov model. Updating flow values greatly affected model predictions. This shows the importance of updating the inlet flow rate, as the Kalman filter assigns the maximum flow allowed into the road to be the inlet flow rate until the next filter iteration. Updates to density produce temporary effects in the model estimates, and was not as important in updating the model.

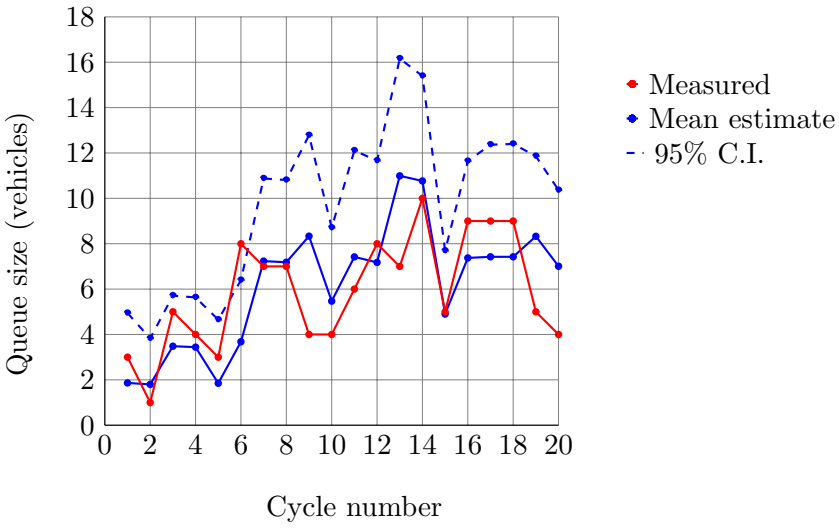

(a) $\ell_i = 15.55$m, 16 queues in estimated C.I. for $\Delta t \leq \frac{1}{2}$CFL condition

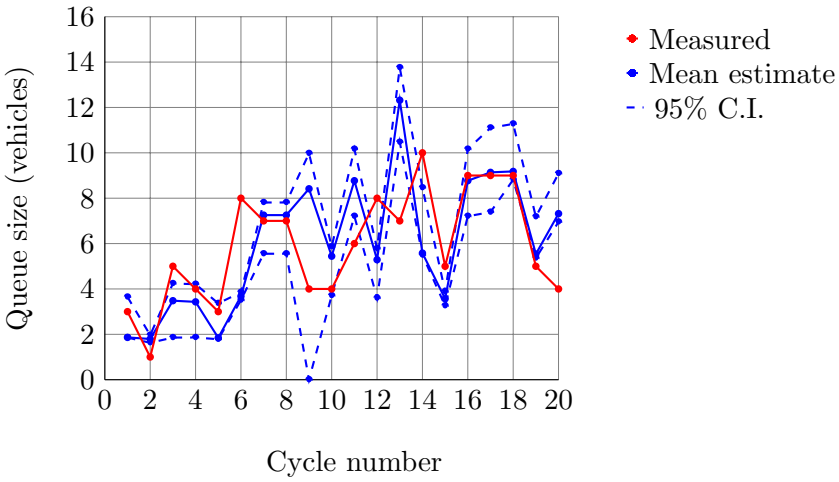

(b) $\ell_i = 15.55$m, 10 queues in estimated C.I. for $\Delta t \leq \frac{1}{16}$CFL condition

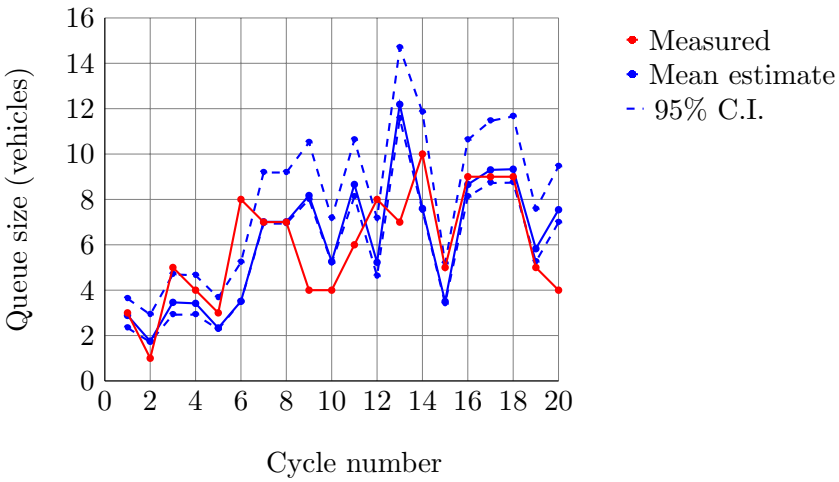

(c) $\ell_i = 4.88$m, 10 queues in estimated C.I. for $\Delta t \leq \frac{1}{2}$CFL condition

Figure 6.: Comparison between estimated and measured queue sizes

5. Conclusion

Macroscopic models accumulate random microscopic phenomenon across lengths of roads. Stochastic models have been developed to simulate the stochastic nature of vehicle interactions and arrivals. In order to produce computationally viable models, researchers have added Gaussian noise to a deterministic model to create a stochastic model. This could lead to negative estimated densities, which is an undesirable physical feature. The model outlined in (Jabari and Liu 2012) creates a doubly stochastic Poisson counting process based on stochastic time headways. This model was developed to create a stochastic cell transmission model with the limiting features of the stochastic process to be the deterministic Godunov scheme. The deviance between the stochastic and deterministic model is derived as a stochastic differential equation, from which the variance of the mean counting process is derived. This stochastic differential equation is shown to be a Gaussian distribution about the fluid limit.

This paper implements the Gaussian approximation model proposed in (Jabari and Liu 2013) on an arterial road in Brookings, SD. The deterministic model is computationally viable, its variance is controllable such that non-negative density distributions are obtainable, and the mean of the original stochastic model used in the derivation of the Gaussian approximation converges in the fluid limit to Godunov scheme dynamics. The linearity of the model allows for the use of Kalman filtering for calibrating the model to real-time data.

The case study was able to produce results with 80% accuracy in predicting observed queue sizes within the confidence interval at the loss of guaranteeing non-negative densities. In practice, it does not seem reasonable to expect that a model maintaining non-negative densities with 95% confidence produces a large variance. It must be determined which takes priority in modeling traffic flow: providing ranges of traffic flow values that accurately represent the modeled situation, or maintaining physical phenomenon that densities should be non-negative.

5.1. *Future work*

The Gaussian approximation model can be applied to any traffic operations management systems which require traffic predictions. This includes advanced signal timing, ramp metering, and advanced wait time notice.

The cell transmission model was developed to solve the LWR model for complicated network topologies. Thus the Gaussian approximation could be investigated and developed for these scenarios. To do this, one would derive this from deterministic merge and diverge dynamics.

It would be of interest for those implementing this model in the future to use Monte Carlo simulation of the stochastic process to check whether the 95% confidence interval about the mean is valid for various time steps. The authors of this paper assumed the derivation of the variance of the stochastic process to its mean to be sufficient.

References

Cambridge Systematics, Inc., and Texas Transportation Institute. 2005. *Traffic congestion and reliability: trends and advanced strategies for congestion mitigation.* Technical report. Federal Highway Administration (FHWA).

Currin, T. R. 2001. *Introduction to traffic engineering: a manual for data collection and Analysis.* Brooks/Cole.

Daft Logic. 2014. "Distance Calculator." Accessed June 2014. http://tinyurl.com/pdudavo.

Daganzo, C. 1994. "The cell transmission model: A dynamic representation of highway traffic consistent with the hydrodynamic theory." *Transportation Research-B* 28 (4): 269–287.

Daganzo, C. 1995. "The cell transmission model: Network traffic." *Transportation Research-B* 29 (2): 79–93.

Godunov, S. 1959. "A difference scheme for numerical solution of discontinuous solution of hydrodynamic equations.." *Matematicheskii Sbornik* 89 (3): 271–306.

Jabari, S., and H. Liu. 2012. "A stochastic model of traffic flow: Theoretical foundations." *Transportation Research Part B* 46 (1): 156–174.

Jabari, S., and H. Liu. 2013. "A stochastic model of traffic flow: Gaussian approximation and estimation." *Transportation Research Part B* 47: 15–41.

Kim, T., and H.M. Zhang. 2008. "A stochastic wave propagation model." *Transportation Research Part B* 42 (7): 619–634.

Leveque, R. J. 1992. *Numerical methods for conservation laws*. Vol. 132. Springer.

Lighthill, M. L., and G. Whitham. 1955. "On kinematic waves. II: A theory of traffic flow on long crowded roads." *Proceedings of the Royal Society of London. Series A. Mathematical and Physical Sciences* 317–345.

Richards, P. I. 1956. "Shockwaves on the highway." *Operations Research* 4: 42–51.

Sumalee, A., R.X. Zhong, T.L. Pan, and W.Y. Szeto. 2011. "Stochastic cell transmission model (SCTM): a stochastic dynamic traffic model for traffic state surveillance and assignment." *Transportation Research Part B* 45 (3): 507–533.